Synthesis of ErBa$_2$Cu$_3$O$_{7-\delta}$ Superconductor Solder for the Fabrication of Superconducting Joint between Gdba$_2$cu$_3$o$_{7-\delta}$ Coated Conductor

Zili Zhang [1], Lei Wang [1], Jianhua Liu [1] and Qiuliang Wang [1,2,*]

[1] Institute of Electrical Engineering, Chinese Academy of Sciences, Beijing 100190, China; zilizhang0816@vip.126.com (Z.Z.); wanglei@mail.iee.ac.cn (L.W.); liujianhua@mail.iee.ac.cn (J.L.)

[2] University of Chinese Academy of Sciences, Beijing 100049, China

[*] Correspondence: qiuliang@mail.iee.ac.cn

Abstract: ErBa$_2$Cu$_3$O$_{7-\delta}$ (Er123) superconductor is one of the best candidates of superconductor solder for the fabrication of superconducting joint between GdBa$_2$Cu$_3$O$_{7-\delta}$ (Gd123) coated conductor, due to its high T_c value (93 K) and highest optimized oxygen annealing temperature among RE123 compounds. In this paper, we systematically research the effect of sintering parameters on the phase formation, microstructure and superconducting properties of Er123 powder. The optimized synthesis route to acquire high purity Er123 powder with as good superconducting properties as Gd123 has been uncovered. The melt temperature of Er123 with different dopant compared to Gd123 is also investigated, and the feasible operating temperature range of Er123 superconductor solder is discussed. This work reveals a very important starting point on fabrication high-quality superconducting joint between the commercial Gd123 coated conductor, which can further improve the development of the persistent operating mode on ultra-high field nuclear magnetic resonance and magnetic resonance imaging.

Keywords: Er123; melt temperature; superconducting solder; superconducting joint

1. Introduction

REBa$_2$Cu$_3$O$_{7-\delta}$ (REBCO) has been considered to be one of the promising superconductors for the insert coil of ultra-high field nuclear magnetic resonance and magnetic resonance imaging [1–5]. The RIKEN has successfully fabricated an NMR by REBCO operated in the driven mode and demonstrated high-resolution NMR spectra [6]. In the real application, the persistent mode is preferred to reduce the heat leak and get a more stable magnetic field. One of the key points of persistence mode is a superconducting joint between REBCO coated conductor with resistance less than 10^{-12} Ω [7]. However, most joints now are on the level 10^{-8} to 10^{-9} Ω [8–10], which indicates that a feasible superconducting joint fabrication process is still required.

The first persistent current joint between REBCO was invented by Park et al. in 2014 [11]. The GdBa$_2$Cu$_3$O$_{7-\delta}$ (Gd123) coated conductor was directly connected by long time heat treatment to diffuse the Gd123 to each other. After over 350 h oxygen annealing, the final joint had a critical current of 84 A and a resistance less than 10^{-17} Ω. Although the properties fit the application criterion of the persistent mode, the too long annealing time is not feasible in the real application. In 2015, the Jin et al. in RIKEN established a novel method called crystalline joint by a melted bulk (CJMB). Two untouched Gd123 coated conductors were put on a RE123 bulk with low melt temperatures such as YBa$_2$Cu$_3$O$_{7-\delta}$ (Y123) and YbBa$_2$Cu$_3$O$_{7-\delta}$ (Yb123) [12,13]. After ingeniously designed the heat treatment, the Y123 melt and regrow to form a superconductor joint between Gd123 coated conductors. The annealing

time was successfully reduced to only 72 h with a final resistance of 8×10^{-13} Ω. The core idea of this method is using low melt temperature REBCO materials as the superconducting solder.

Using low melt temperature REBCO as a superconducting solder has also been used in joining Y123 single domain bulks [14–18]. In all these researches, appropriate oxygen annealing is essential to achieve high supercurrent capability [19]. In particular, $ErBa_2Cu_3O_{7-\delta}$ (Er123) has the highest optimized annealing temperature among RE123 compounds, which is strongly suggesting a drastic decrease in annealing time for the accomplishment of an optimally carrier-doped condition in Er123 compounds due to the large diffusion coefficient of oxygen [20]. There are only a few reports mentioned on Er123 powder [21–26], and none of them has systematic research on the synthesis of such compounds. The reported synthesis temperature even has some tens of degrees difference, which brings big confusion to other researchers.

In this paper, we systematically investigate the effect of synthesis parameters on the phase formation, microstructure and superconducting properties. High purity Er123 powder with high supercurrent capability is acquired. The melt temperature of Er123 and Gd123 with different dopants are also researched.

2. Materials and Methods

Powder Preparation. The Er123 powders were synthesized by the solid reaction method. The Er_2O_3 (99.9% Aladdin), $BaCO_3$ (99.9% Aladdin) and CuO powder (99.99% Aladdin) powder were mixed in stoichiometric ratio to form Er123. The powders were mixed, ground together, and pressed into a pellet that was put into a tube furnace and heat-treated at different temperatures for 24 h under flowing O_2. For the multiple sintering sample, the product powders were ground, pressed and heat-treated again under the same process. The Er211 powders were synthesized by a similar process with the sintering parameters of 1000 °C for 24 h under the flow Ar. The oxygen annealing process used the Er123 sample with the highest purity. The as-synthesized powders were ground and pressed to pellet. The pellet was put into a tube furnace and heat-treated at 500 °C for 24 h or 48 h under flowing O_2 with a large flow rate. The commercial Gd123 powder is coming from Shanghai Superconductor Technology Co., Ltd.

Sample Characterization. The phase analysis of the samples was characterized by Cu Kα x-ray diffraction (XRD, Burker D8), and the grain sizes were calculated by using the Debye–Scherrer formula. Microstructures were observed by scanning electron microscopy (SEM, FEI Quanta 450) with Energy Dispersive X-Ray Spectroscopy (EDX). The melt temperature was measured by differential thermal analysis (DTA-TGA, TA Instruments 2960) at a heating rate of 10 °C/min in the Air. Magnetic measurements were performed at 5K and 77 K in a vibrating sample magnetometer (VSM) using a Physical Properties Measurement System (PPMS) from Quantum Design Ltd. under an applied field up to 7 T. Field-cooled (FC) and the zero-field-cooled (ZFC) curve was measured in an applied field of 10 mT. Magnetization values were determined from the measured magnetic moment using the sample mass and nominal density ρ = (Gd123: 6.384 g/cm^3, Er123: 7.152 g/cm^3) to calculate the actual volume of material present. The critical current densities, J_c (in Am^{-2}), of the samples were calculated by applying a standard Bean model expression for spherical grains to magnetic hysteresis loops through the formula:

$$\Delta M = \frac{1}{3}\frac{w}{2}J_c\left(1 - \frac{w}{3l}\right)$$

where ΔM (in Am^{-1}) is the vertical width of the magnetization loop and $l \geq w >> t$ (in m) are the dimensions of individual plate-like crystallites in the samples. This formula was derived in Reference [27] for a collection of randomly-oriented thin platelets of an anisotropic superconductor such as REBCO, and yields an estimate of the *ab*-plane J_c for fields applied parallel to c typically accessed in transport measurements while incorporating considerations relating to the anisotropy of the superconductor, the geometry of the crystallites, their respective orientations to the applied field and demagnetization effects. In the case of the commercial Gd123 powder, the standard Bean model expression for spherical grains $\Delta M = d/3 J_c$ has been used, where d is the grain diameter (taken as 5 μm).

3. Results

Figure 1a shows the XRD results of the sample sintered at different temperatures for 24 h. All the samples consist of Er123 as a domain phase with impurities of Er_2BaCuO_5 (Er211) and $BaCuO_2$. It shows that the sintering temperature has an apparent effect on the phase formation. As shown in Figure 1b, along with the temperature raising to 920 °C, the peak intensity of Er123 kept increasing, at the same time the Er211 peak became weaker. When the temperature reaches 930 °C, such a trend reversed. The grain size calculated from XRD results shows the same evolution trend with the Er123 peak intensity.
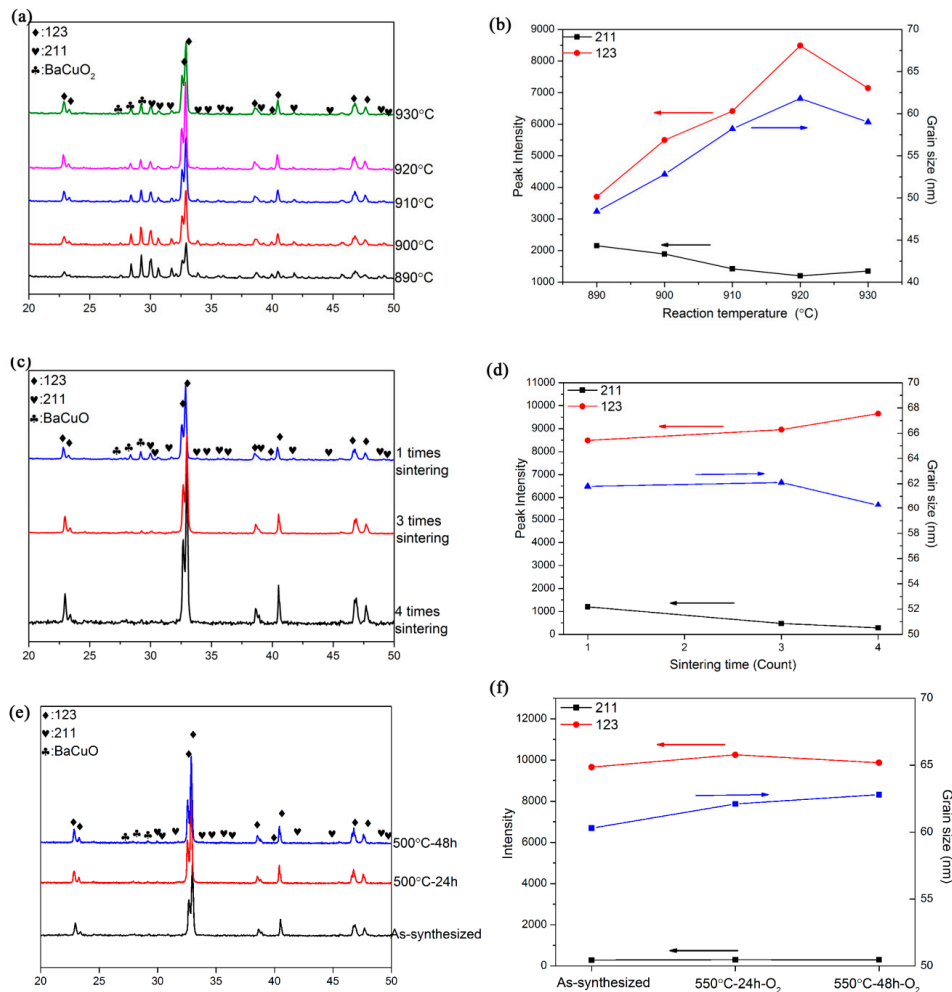

Figure 1. (**a**) phase formation of Er123 sintered by different temperature for 24 h; (**b**) Peak intensity and grain size from the XRD results of Er123 sintered by different temperature for 24 h; (**c**) phase formation of Er123 sintered at 920 °C for 24 h by multiple times; (**d**) Peak intensity and grain size from the XRD results of Er123 sintered at 920 °C for 24 by multiple times; (**e**) phase formation of Er123 with oxygen annealing at 500 °C for 24~48 h; (**f**) Peak intensity and grain size from the XRD results of Er123 with oxygen annealing at 500 °C for 24~48 h.

Multiple heat treatment is the conventional method to improve the reaction in the solid reaction method. The multiple heat treatment under 920 °C has been attempted, as shown in Figure 1c,d. The impurity phase such as Er211 and $BaCuO_2$ nearly disappeared after 4 times sintering. Additionally, the grain size does not have significant changing along with the multiple heat treatment.

The purpose of oxygen annealing on the REBCO powder is to compensate for the oxygen deficiency brought by the high temperature heat treatment, the annealing at 500 °C for 24 and 48 h was also

tried. As shown in Figure 1e,f, the change of phase formation and grain size before and after oxygen annealing is negligible, which both have high purity Er123 as the dominant phase.

Figure 2 shows the SEM images of the sample sintered at different temperatures for 24 h. When the temperature was 890 °C, there are plenty of small round particles embedded inside big Er123 particles, as pointed by the red arrow. The EDX results showed that these small particles are the Er211 phase. As the temperature rose, these small round particles gradually disappeared. When the temperature reaches the range of 910~920 °C, only the morphology of big plate-like particles can be found. However, the big plate-like particles started to disassemble at a temperature of 930 °C. This is due to the reaction between the Er123 and CuO to form Er211 and liquid phase [28]. Combined with the XRD results, we think it is due to the decomposition of Er123 to Er211 at the excessive temperature. However, we did not find the small round Er211 particles as in the sample of 890 °C. We randomly chose 50 particles and measured the particle size of the plate-like Er123. The average particles size of the Er123 in the sample of 900~920 °C are 5 μm × 5 μm × 1 μm. The particle size has a small change in the sample of 890 °C and 930 °C, due to the existence of Er211 impurities. However, the same value will be used in the calculation of the Bean model.
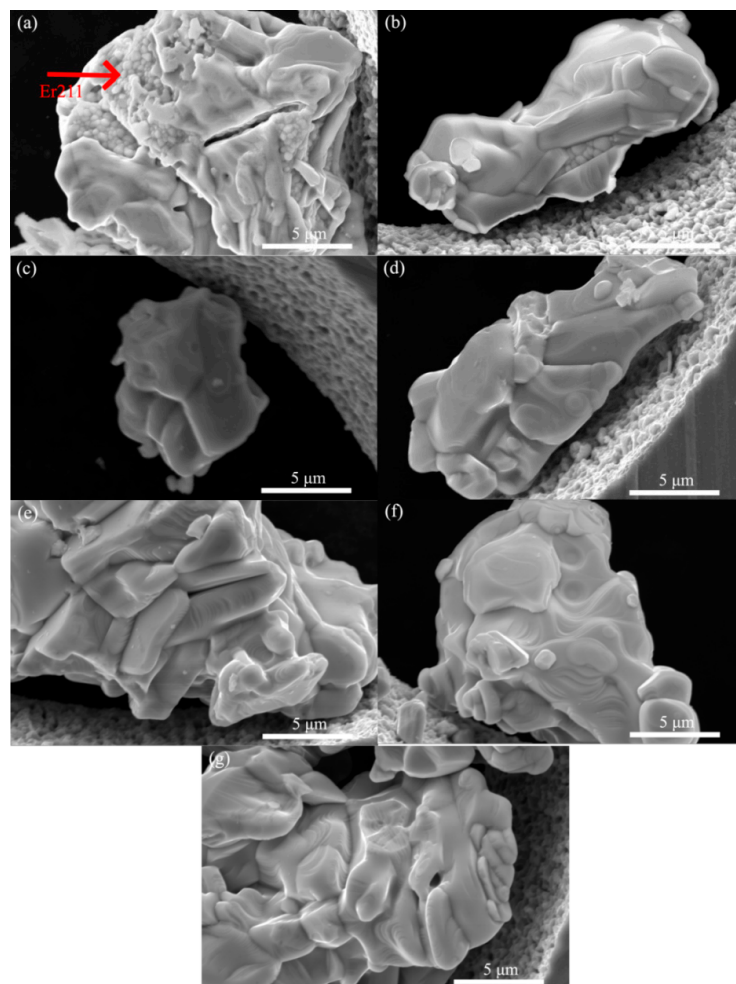

Figure 2. The SEM images of Er123 powder after different sintering. (**a**): 890 °C for 24 h; (**b**): 900 °C for 24 h; (**c**): 910 °C for 24 h; (**d**): 920 °C for 24 h; (**e**): 920 °C for 24 h (three times); (**f**): 920 °C for 24 h (four times); (**g**): 930 °C for 24 h.

We did multiple heat treatment on the sample of 920 °C. Although the phase purity was further improved, there was no apparent change in the microstructure, as shown in Figure 2e,f. The grain size also did not change after multiple heat treatment. The microstructure and particle size of the sample

with four times sintering at 920 °C for 24 h and oxygen annealing at 500 °C for 48 h are nearly the same as the sample with only one-time sintering at 920 °C for 24 h. It indicates that the Er123 particle with a size around 5μm is very stable, which is hard to connect together under more heat treatment.

Figure 3 shows the superconducting properties of the sample sintered with different parameters. As shown in Figure 3a, under different sintering temperatures, the $T_{c\,onset}$ value is nearly the same—around 91 K—but there is an apparent difference in the magnetization value. In both the ZFC and FC curves, the magnetization value kept increasing and reached the maximum at 920 °C. The ZFC value shows how many superconductor phases in the sample. That is the reason the magnetization value in the ZFC curve has exactly the same trend as the peak intensity of Er123. The FC magnetization value is associated with the Meissner fraction, and is much lower in magnitude for both samples, indicating flux trapping within the grains. The increasing FC magnetization value indicates the poor pinning in all the samples. All the J_c curves of the sample with different sintering temperatures are parallel to each other at 5 K up to 7 T, as shown in Figure 3b. The sample of 920 °C has the highest J_c value, which is due to the highest Er123 phase amount. The 211 phase is the most conventional pinning center in the REBCO bulks. However, although there is a visible Er211 phase in both the sample of 890 °C and 930 °C, we did not find any better field performance in these two samples.
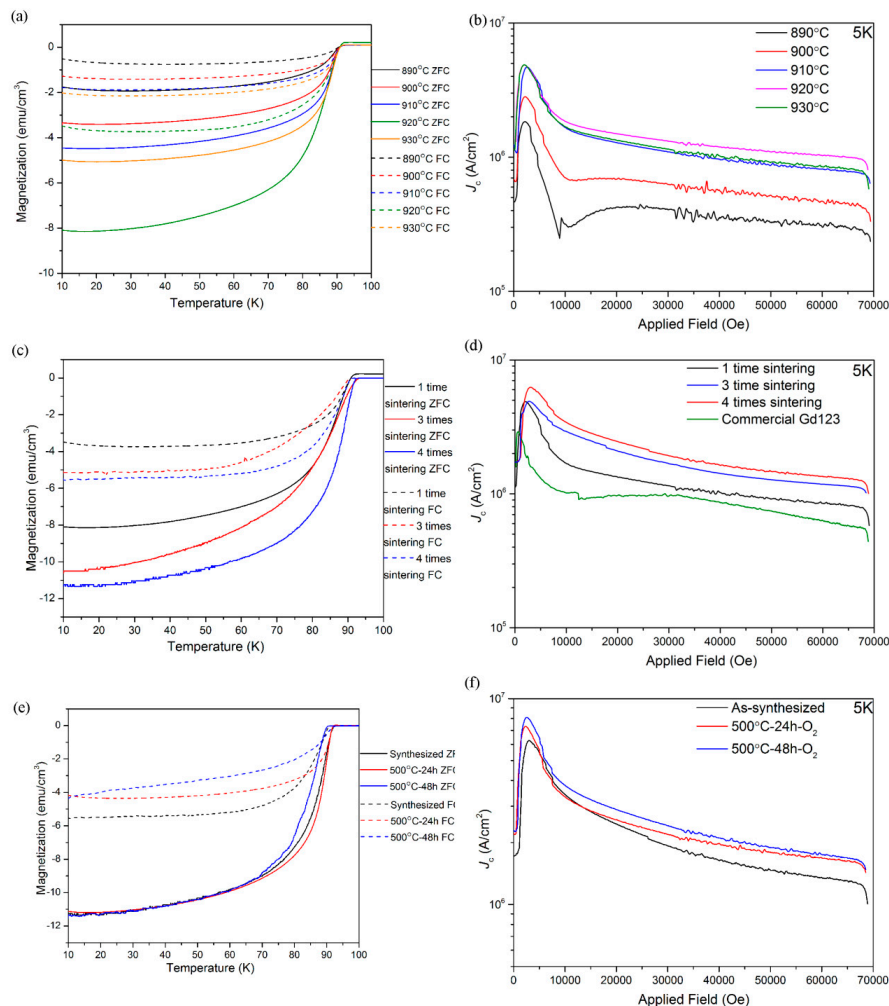

Figure 3. (**a**) ZFC and FC curves of the Er123 sintered by different temperature for 24 h; (**b**) J_c vs B curve at 5 K of the Er123 sintered by different temperature for 24 h; (**c**) ZFC and FC curves of the Er123 sintered at 920 °C for 24 h by multiple times; (**d**) J_c vs B curve at 5 K of the Er123 sintered at 920 °C for 24 h by multiple times; (**e**) ZFC and FC curves of the Er123 with oxygen annealing at 500 °C for 24~48 h; (**f**) J_c vs B curve at 5 K of the Er123 with oxygen annealing at 500 °C for 24~48 h.

As shown above, the multiple heat treatment at 920 °C can further improve the phase purity. The enhancement of ZFC magnetization value and J_c value also proved such results, as shown in Figure 3c,d. Moreover, the J_c value at 5K is higher than the commercial Gd123 powder at the entire 0~7 T. Since the Gd123 powder is the exact one that Shanghai Superconductor Technology Co., Ltd. used to fabricate Gd123 coated conductor, this result indicates that the Er123 has similar intra-grain supercurrent with Gd123 which is used to fabricate commercial coated conductor. If the excellent texture of Er123 can be obtained between Gd123 commercial coated conductor by exquisitely designing the heat treatment process, we also expect the same level inter grain supercurrent of Er123 to Gd123, which finally provides a possibility to fabricate superconducting joint with high current capability by using Er123 as superconducting solder.

Although the phase formation and microstructure did not change after oxygen annealing, the superconducting properties showed some difference, as shown in Figure 3e,f. After annealing at 500 °C under O_2, the ZFC magnetization values did not have further improvement, indicated that although sintering at 920 °C could cause oxygen deficiency, the cooling underflow oxygen can basically compensate the deficiency. However, the FC magnetization values slightly decreased with the prolonging of the annealing time at 500 °C. The J_c curves also tell a new story: the high filed performance was mildly improved in the sample with oxygen annealing. Both results show that oxygen annealing improves the pinning in the Er123 powder.

4. Discussion

From the results above, it can be found that there is a reversible reaction between Er123 and Er211 phases. At lower temperatures, the Er211 can react with $BaCuO_2$ form Er123, moreover, the Er123 can also decompose to Er211. This is the reason the Er123 intensity has a convex shape with the increasing temperature, and the optimized temperature windows on the Er123 formation is pretty narrow. These Er211 seems to agglomerate to particles of few micrometers and embedded into the large Er123 particles. According to the superconducting properties, especially the high field performance of J_c value, such embedded Er211 particles could not act as the pinning center but only degrade the T_c value. After multiple heat treatments, the impurity phase such as Er211 can be eliminated; however, the poor pinning problem emerges. Therefore, the controllable Er211 particles which can act as pinning centering are essential to the Er123 as the superconducting solder. We successfully synthesized the high purity Er211 phase with a particle size of around 10 micrometers, as shown in Supplementary Materials Figure S1. However, simply mixing such Er211 will not bring the pinning center, and further refining work is necessary.

During recent decades, research on the melt texture synthesis of REBCO single domain bulk, multiple additives has proved that it is a benefit to the superconducting properties of the final products. Typically, the Ag or Ag_2O is added to improve the connectivity and decrease the melt temperature of REBCO [29–32], which brings lower heat treatment temperature. Pt is also a common additive, which can inhibit the growth of the 211 phase [33,34]. The large 211 particles can lead to an inhomogeneous reaction. All these beneficial dopants will be introduced in the fabrication of a superconducting joint by using Er123 as a superconducting solder. Therefore, the effect of such additives on the Er123 melt temperature is critical, which directly determines the heat treatment process of fabrication of the superconducting joint.

After obtaining Er123 powder with high purity and high supercurrent capability, the feasibility of Er123 as a superconducting solder is discussed here. Since the REBCO need the biaxial texture to carry high supercurrent, the only method of fabricating a superconducting joint between REBCO coated conductor is using REBCO materials to form a texture joint. In the most conventional method, the REBCO powder of low melt temperature is added as a superconducting solder between the REBCO coated conductor. During the heat treatment, the solder REBCO melts but the REBCO coated conductor keeps inert. After cooling at a slow rate, the solder REBCO grows to texture form based on the REBCO coated conductor. Therefore, the low melting temperature of superconducting solder is critical.

Figure 4 shows the DTA results of the Er123 powder and Gd123 powder with a different dopant in Air. It is found that the melt temperature of Er 123 decreased about 30 °C by adding Ag and Ag_2O, but no such effect is found in the curve of Pt adding. The melt temperature decreasing by adding Ag and Ag_2O is very useful, which may bring more safety margins when designing the heat treatment process of the superconducting joint.
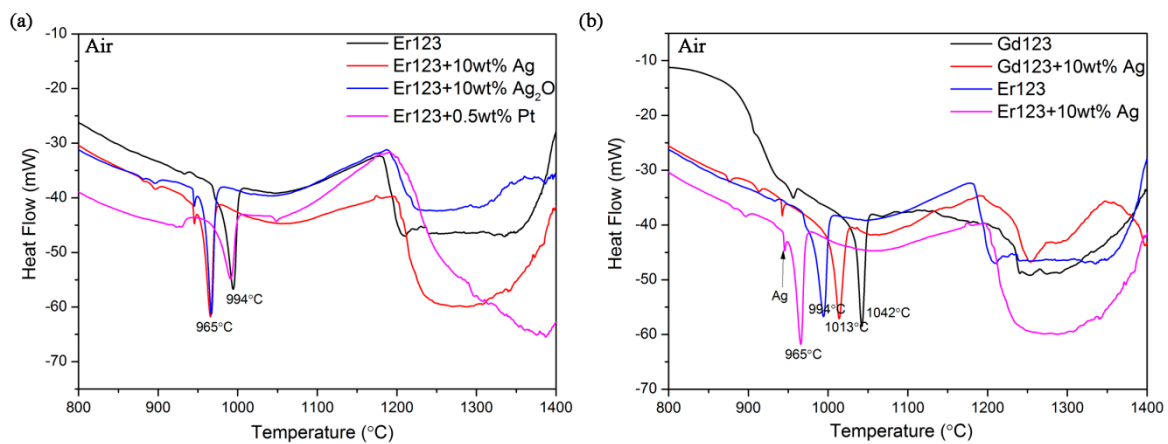

Figure 4. (**a**) The DTA results of Er123 powder with different dopants; (**b**) The DTA results of Er123 and Gd123 powder with and without Ag doping.

However, according to our previous study, the Ag can decrease the melt temperature of REBCO by just contacting instead of homogenous mixing [35]. In the report, we found that the Ag can decrease the melt temperature of Yb123 to the same level as the Yb123 powder mixed with Ag. So if the Ag is added to Er123 during the fabrication of the superconducting joint between the G123 coated conductor, the effect of Ag on the melt temperature of Gd123 should be considered. Figure 4b shows the DTA results of the Er123 and Gd123 powder with and without Ag adding. It is found that the melt temperatures of both theGd123 and Er123 were decreased by the same level (about 29 °C) with Ag adding. So the heat treatment temperature range moved from 994~1042 °C to 965~1013 °C without any expansion. For safety reasons, the maximum heat treatment temperature should set below 1013 °C instead of 1042 °C, in case of the melting of Gd123 under the effect of Ag.

5. Conclusions

The synthesis parameters of Er123 powder were systematically optimized. The optimization temperature was 920 °C; both higher or lower temperatures brought small Er211 particles embedded in Er123 plate-like particles. The Er211 phase is a kind of barrier of the flow superconducting current but cannot act as a pinning center. After multiple sintering processes, high purity Er123 powder with as good superconducting properties as Gd123 coated conductor was acquired. The extra oxygen annealing at 500 °C is not necessary for this synthesis method. The melt temperature of Er123 and Gd123 with different dopants were also investigated. After adding Ag or Ag_2O, a feasible operating temperature range (965~1013 °C) is uncovered, at which the superconducting solder Er123 can melt but the Gd123 in coated conductor remains inert. This shows the important first step to obtain a superconducting joint with high current capability.

Author Contributions: Z.Z. contributed to the main part of this article including investigation, analysis and original writing. The L.W., J.L. and Q.W. contributed to the supervision of the investigation and writing—review and editing.

References

1. Iwasa, Y.; Bascnan, J.; Hahn, S.; Yao, W. High-temperature superconductors for NMR/MRI magnets: Opportunities and challenges. *Prog. Supercond. Cryog.* **2009**, *11*, 1–7.
2. Yanagisawa, Y.; Piao, R.; Iguchi, S.; Nakagome, H.; Takao, T.; Kominato, K.; Hamada, M.; Matsumoto, S.; Suematsu, H.; Jin, X. Operation of a 400MHz NMR magnet using a (RE:Rare Earth)Ba$_2$Cu$_3$O$_{7-x}$ high-temperature superconducting coil: Towards an ultra-compact super-high field NMR spectrometer operated beyond 1GHz. *J. Magn. Reson.* **2014**, *249*, 38–48. [CrossRef] [PubMed]
3. Iwasa, Y.; Bascunan, J.; Hahn, S.; Voccio, J.; Kim, Y.; Lecrevisse, T.; Song, J.; Kajikawa, K. A High-Resolution 1.3-GHz/54-mm LTS/HTS NMR Magnet. *IEEE Trans. Appl. Supercond.* **2015**, *25*, 4301205. [CrossRef]
4. Tosaka, T.; Miyazaki, H.; Iwai, S.; Otani, Y.; Takahashi, M.; Tasaki, K.; Nomura, S.; Kurusu, T.; Ueda, H.; Noguchi, S.; et al. R&D Project on HTS Magnets for Ultra high-Field MRI Systems. *IEEE Trans. Appl. Supercond.* **2016**, *26*, 4402505.
5. Yokoyama, S.; Lee, J.; Imura, T.; Matsuda, T.; Eguchi, R.; Inoue, T.; Nagahiro, T.; Tanabe, H.; Sato, S.; Daikoku, A.; et al. Research and Development of the High Stable Magnetic Field ReBCO Coil System Fundamental Technology for MRI. *IEEE Trans. Appl. Supercond.* **2017**, *27*, 4400604. [CrossRef]
6. Piao, R.; Iguchi, S.; Hamada, M.; Matsumoto, S.; Suematsu, H.; Saito, A.T.; Li, J.; Nakagome, H.; Takao, T.; Takahashi, M.; et al. High resolution NMR measurements using a 400 MHz NMR with an (RE)Ba$_2$Cu$_3$O$_{7-x}$ high-temperature superconducting inner coil: Towards a compact super-high-field NMR. *J. Magn. Reson.* **2016**, *263*, 164–171. [CrossRef] [PubMed]
7. Swenson, C.A.; Markiewicz, W.D. Persistent joint development for high field NMR. *IEEE Trans. Appl. Supercond.* **1999**, *9*, 185–188. [CrossRef]
8. Kim, Y.; Bascunan, J.; Lecrevisse, T.; Hahn, S.; Voccio, J.; Park, D.K.; Iwasa, Y. YBCO and Bi2223 coils for high field LTS/HTS NMR magnets: HTS-HTS joint resistivity. *IEEE Trans. Appl. Supercond.* **2013**, *23*, 6800704.
9. Baldan, C.A.; Oliveira, U.R.; Bernardes, A.A.; Oliveira, V.P.; Shigue, C.Y.; Ruppert, E. Electrical and superconducting properties in lap joints for YBCO tapes. *J. Supercond. Nov. Magn.* **2013**, *26*, 2089–2092. [CrossRef]
10. Walsh, R.P.; McRae, D.; Markiewicz, W.D.; Lu, J.; Toplosky, V.J. The 77-K stress and strain dependence of the critical current of YBCO coated conductors and lap joints. *IEEE Trans. Appl. Supercond.* **2012**, *22*, 8400406. [CrossRef]
11. Park, Y.; Lee, M.; Ann, H.; Choi, Y.K.; Lee, H. A superconducting joint for GdBa$_2$Cu$_3$O$_{7-\delta}$ coated conductors. *NPG Asia Mater.* **2014**, *6*, e98. [CrossRef]
12. Jin, X.Z.; Yanagisawa, Y.; Maeda, H.; Takano, Y. Development of a superconducting joint between a GdBa2Cu3O7-δ-coated conductor and YBa$_2$Cu$_3$O$_{7-\delta}$ bulk: Towards a superconducting joint between RE (Rare Earth) Ba$_2$Cu$_3$O$_{7-\delta}$-coated conductors. *Supercond. Sci. Technol.* **2015**, *28*, 075010. [CrossRef]
13. Jin, X.Z.; Yanagisawa, Y.; Maeda, H. Measurement of Persistent Current in a Gd123 Coil with a Superconducting Joint Fabricated by the CJMB Method. *IEEE Trans. Appl. Supercond.* **2018**, *28*, 4602604. [CrossRef]
14. Noudem, J.G.; Reddy, E.S.; Tarka, M.; Noe, M.; Schmitz, G.J. Melt-texture joining of YBa$_2$Cu$_3$O$_y$ bulks. *Supercond. Sci. Technol.* **2001**, *14*, 363–370. [CrossRef]
15. Mukhopadhyay, S.M.; Mahadev, N.; Sengupta, S. Microstructural and spectroscopic analyses of a strongly-linked joint formed in a superconductor. *Physica C* **2000**, *329*, 95–101. [CrossRef]
16. Zheng, H.; Jiang, M.; Nikolova, R.; Welp, U.; Paulikas, A.P.; Huang, Y.; Crabtree, G.W.; Veal, B.W.; Claus, H. High critical current "weld" joints in textured YBa$_2$Cu$_3$O$_x$. *Physica C* **1999**, *322*, 1–8. [CrossRef]
17. Schmitz, G.J.; Tigges, A.; Schmidt, J.C. Microstructural aspects of joining superconductive components using (RE)Ba$_2$Cu$_3$O$_{7-x}$ solder. *Supercond. Sci. Technol.* **1998**, *11*, 73–75. [CrossRef]
18. Azoulay, J. YBCO thin film evaporation on as-deposited silver film on MgO. *Physica C* **1999**, *324*, 187–192. [CrossRef]

19. Shimoyama, J.I.; Horii, S.; Otzschi, K.; Kishio, K. How to optimize critical current performance of RE123 materials by controlling oxygen content. *Mater. Res. Soc. Symp. Proc.* **2002**, *689*, 265–269. [CrossRef]

20. Horii, S.; Ichinose, A.; Mukaida, M.; Matsumoto, K.; Ohazama, T.; Yoshida, Y.; Shimoyama, J.I.; Kishio, K. Enhancement of Critical Current Density in $ErBa_2Cu_3O_y$ Thin Films by Post-Annealing. *Jpn. J. Appl. Phys.* **2004**, *43*, L1223–L1225. [CrossRef]

21. Iida, K.; Yoshioka, J.; Sakai, N.; Murakami, M. Superconducting joint of Y–Ba–Cu–O superconductors using Er–Ba–Cu–O solder. *Physica C* **2002**, *370*, 53–58. [CrossRef]

22. Nakashima, T.; Maruyama, T.; Honzumi, M.; Horii, S.; Shimoyama, J.; Kishio, K. Relationship between Critical Current Properties and Microstructure of Er123 Melt-Solidified Bulks. *IEEE Trans. Appl. Supercond.* **2005**, *15*, 3176–3179. [CrossRef]

23. Kita, R.; Hosoya, N.; Otawa, N.; Kawabata, S.; Nakamura, T.; Miura, O.; Mukaida, M.; Yamada, K.; Ichinose, A.; Matsumoto, K.; et al. Effects of RE_2O_3 (RE = Tm, Sc, Yb) addition on the superconducting properties of $ErBa_2Cu_3O_y$. *Physica C* **2009**, *469*, 1157–1160. [CrossRef]

24. Yoshioka, J.; Iida, K.; Negichi, T.; Sakai, N.; Noto, K.; Murakami, M. Joining Y123 bulk superconductors using Yb–Ba–Cu–O and Er–Ba–Cu–O solders. *Supercond. Sci. Technol.* **2002**, *15*, 712–716. [CrossRef]

25. Iida, K.; Kono, T.; Kaneko, T.; Katagiri, K.; Sakai, N.; Murakami, M.; Koshizuka, N. Joining of Y–Ba–Cu–O/Ag bulk superconductors using Er–Ba–Cu–O/Ag solder. *Supercond. Sci. Technol.* **2004**, *17*, S46–S50. [CrossRef]

26. Iida, K.; Yoshioka, J.; Negichi, T.; Noto, K.; Sakai, N.; Murakami, M. Strong coupled joint for Y–Ba–Cu–O superconductors using a sintered Er–Ba–Cu–O solder. *Physica C* **2002**, *378–381*, 622–626. [CrossRef]

27. Peterson, R.L. Magnetization of Anisotropic Superconducting Grains. *J. Appl. Phys.* **1990**, *67*, 6930–6933. [CrossRef]

28. MacManus-Driscoll, J.L. Materials Chemistry and Thermodynamics of $REBa_2Cu_3O_{7-x}$. *Adv. Mater.* **1997**, *9*, 457–473. [CrossRef]

29. Diko, P.; Fuchs, G.; Krabbes, G. Influence of silver addition on craking in melt-grown YBCO. *Physica C* **2001**, *363*, 60–66. [CrossRef]

30. Ates, A.; Yanmaz, E. The effects of Ag addition and magnetic field on melt-processed $YBa_2Cu_3O_x$ superconductors. *J. Alloys Comp.* **1998**, *279*, 220–228. [CrossRef]

31. Cakir, B.; Aydiner, A. Structural and magnetic properties of the ring shaped 40 wt% Y211 added TSMG Y123 bulk superconductors welded by Ag2O added MPMG YBCO solder material. *J. Mater. Sci. Mater. Electron.* **2017**, *28*, 17098–17106. [CrossRef]

32. Diko, P.; Krabbes, G.; Wende, C. Influence of Ag addition on crystallization and microstructure of melt-grown single-grain $YBa_2Cu_3O_7$ bulk superconductors. *Supercond. Sci. Technol.* **2001**, *14*, 486–495. [CrossRef]

33. Manton, S.J.; Beduz, C.; Yang, Y.F. Rejoining of Single Grain Melt Textured Bulk YBazCu30,-x I. *IEEE Trans. Appl. Supercond.* **1999**, *9*, 2089–2092. [CrossRef]

34. Zhou, L.; Chen, S.K.; Wang, K.G.; Wu, X.Z.; Zhang, P.X.; Feng, Y.; Wen, H.H.; Li, S.L. Preparation of enhanced Jc YBCO bulks by powder melting process with a combination of submicron 211 precursor and Pt addition. *Physica C* **2002**, *371*, 62–68. [CrossRef]

35. Zhang, Z.; Jiang, J.; Tian, H.; Wang, Q.; Larbalestier, D.; Hellstrom, E. Investigation of the melt-growth process of $YbBa_2Cu_3O_{7-\delta}$ powder in Ag-sheathed tapes. *CrystEngComm* **2019**, *21*, 1369–1377. [CrossRef]